Desalination and Water Treatment
www.deswater.com

doi: 10.5004/dwt.2017.21260

85 (2017) 237–249
August

The removal of methyl orange by nanohydroxyapatite from aqueous solution: isotherm, kinetics and thermodynamics studies

M. Lakrat[a], K. Azzaoui[a,*], S. Jodeh[b,*], N. Akartasse[a], E. Mejdoubi[a], A. Lamhamdi[a,c], M. Berrabah[a], O. Hamed[b], B. Razzouki[d], M. Algarra[e]

[a]*Laboratory LMSAC, Faculty of Sciences, Mohamed 1st University, P.O. Box 717, Oujda 60000, Morocco, Tel. +212677042082; emails: k.azzaoui@yahoo.com (K. Azzaoui), meddlakrati@gmail.com (M. Lakrat), nakkartasee@yahoo.fr (N. Akartasse), ee.mejdoubi@gmail.com (E. Mejdoubi), abdellatiflamhamdi@hotmail.com (L. Lamhamdi), berrabah.mohamed@laposter.net (M. Berrabah)*
[b]*Department of Chemistry, An-Najah National University, P.O. Box 7, Nablus, Palestinian Authority, Tel. +970599590498; emails: sjodeh@hotmail.com (S. Jodeh), ohamed@najah.edu (O. Hamed)*
[c]*National School of Applied Sciences Al Hoceima, Mohamed 1st University, P.O. Box 717, Oujda 60000, Morocco*
[d]*Department of Chemistry, LS3ME, Faculty of Sciences, University Mohammed V, Rabat, Morocco, email: brazzouki@yahoo.fr*
[e]*Department of Inorganic Chemistry, Faculty of Science, University of Malaga, Spain, email: malgarra67@gmail.com*

Received 24 January 2017; Accepted 27 July 2017

ABSTRACT

Hydroxyapatite (HAp) is a biomaterial with a large number of useful applications. In this work, a method for the preparation of HAp at nanoscale was developed (nano-HAp). The prepared nano-HAp was used in the extraction of methyl orange (MO) from water. The special chemical composition, the crystal structure of HAp and molecular structure of MO made extraction occurs at a good efficiency. Structure of the prepared HAp was confirmed by powder X-ray diffraction, Fourier transform infrared spectroscopy and scanning electron microscope. Batch experiments were used to evaluate the tendency of the prepared nano-HAp for extracting the MO from water. The effect of temperature, time, pH and the amount of adsorbent on the rate of adsorption were evaluated and found to have a noticeable effect on the adsorption efficiency. The optimum conditions for extraction of MO by nano-HAp were determined. In all runs, in the first 5–15 min of contact time at room temperature the nano-HAp showed the highest rate of adsorption. Then, the rate leveled off after about 20 min. The temperature showed almost directly proportional with the rate of adsorption. The thermodynamic studies revealed a spontaneous nature of adsorption at different temperature.

Keywords: Wastewater; Hydroxyapatite; Methyl orange; Adsorption; Environment

1. Introduction

Discharging of effluents with azo dyes in nature negatively impacts environment and many biological cycles. The issue is becoming more serious, considering the growing world population and the consequent higher demand for clean water [1]. Azo dyes are those contain –N=N– functionality such as for instance methyl orange (MO) and methylene blue. Their stability and their poor biodegradability make their impact on the environment and human indefinite [2]. In addition, some of them are toxic and mutagenic [3]. For this reason, it is necessary that these dyes are removed from water to decolorize it and to prevent their effect on nature from happening. Several treatments have been used to remove these harmful materials from wastewater. The treatments used could be classified into three categories: biological, chemical and physical. Unfortunately, the biological treatment was unsatisfactory; since the composition of these toxic materials is not easily biodegradable. The chemical treatments are economically not viable, since large dose is

* Corresponding author.

required, which may lead to other toxic materials and a large quantity of sludge [4].

However, the physical methods are non-destructive and mainly involved in transferring the dyes from one medium to another. The physical treatment includes adsorption, coagulation, ozone treatment, electro Fenton's, photocatalytic degradation and decolorization with hypochlorite [5–8].

Among the physical treatment, adsorption remains the most widely used process, since it can be easy to implement and at low cost. Various adsorbents were reported in the literature for the removal of dyes from wastewater, in particular activated carbon, which was reported by several researchers [9]. The adsorption of organic molecules such as dyes on activated carbon has proven to be a very effective technique, however, in the case of some recalcitrant dyes; activated carbon overdoses are required for efficiency, making excessive cost of the operation.

Recently, the research focused on surface modification of nanostructured absorbents, by adding a functionality that enhances the efficiency of adsorbent for dyes. Such as for instance modification of glycine [10], gum arabic [11], glutaraldehyde [12], 3-mercaptopropionic acid [13], citric acid [14], poly(acrylic acid) [15], humic acid [16] and bisphenol A [17–22]. It has been found that surface modification of adsorbents serve two purposes: it provides novel binding sites for organic molecules and prevents the adsorbent nanoparticles from forming aggregates which improves the dispersion stability of the adsorbent nanoparticles in suspension medium [9]. Despite the major improvements caused by functionalization, the cost issue and the potential environmental risks that may cause to the environment [22] prevents the surface-modified nanoparticle from being used at an industrial scale. Therefore, a low-cost, environment-friendly and biocompatible nanomaterial-based adsorbent are needed for the removal of organic materials such as MO from wastewater.

For this reason, development of new adsorbents was the subject of several studies in recent years. In this study, a new biosorbent-based hydroxyapatite (HAp) nanomaterial develop at our laboratory is proposed as an effective low-cost alternative for the removal of MO from wastewater.

Dyes are known for their stability and recalcitrant ability, which makes them very dangerous to human health [23], prolonged exposure to azo dyes, increases the risk of cancer diseases. MO is often used as a pH indicator and its range of color change is 3.1–4.4. MO is a water-soluble azo dye, used in textiles, printing, papermaking, pharmaceuticals, food industries, as well as in research laboratories [23]. Therefore, many technologies such as coagulant photocatalysis, ultrafiltration, biological treatment, electrochemical, oxidizing agents and adsorption have been used to deal with this environmental problem. Adsorption is considered to be the simplest and most effective method. Various solid materials such as alginate, activated carbon, chitosan, modified chitosan, polymer resins and ion-exchange membranes were examined as adsorbents. Resins and membranes are known to be the most important adsorbents.

Dyes have been removed using different techniques like photodegradation of dye acridine yellow on the surface of mesoporous films [24,25] and photocatalyst fabrication using method of sol–gel for perovskites photodegradation [26,27]. Other studies were used for the removal of NO_x on TiO_2/MoS_2 nanocomposites [28]. Zare et al. [29] did a review of comparative study on the basis of adsorption capacity between CNTs and activated carbon as adsorbent for removal of noxious synthetic dyes.

The composites of HAp-based were prepared and evaluated by various spectroscopic and analytical techniques [30]. HAp and GA composite is bio-based and have unique properties such as biocompatibility, bioactivity and osteoconductivity. These properties make it attractive for various applications such as metals extractions. The composite was prepared by the solution method. The possibility of using the prepared composite as a based stationary phase for removal of arsenic(III) from wastewater was evaluated. The composite a very promising adsorbent for arsenic(III).

HAp is a non-toxic, biocompatible and biodegradable material. It has gained importance in view of its special chemical composition and crystal structure [20,21]. Its low water solubility, availability at low cost and its high stability against reducing and oxidizing agents made it perfect candidate for use as a replacement for hard tissues and in drug delivery [21].

In this work, a simple and a convenient method for the preparation of nanoparticles of HAp were developed. The produced nanoparticle of HAp was used in the extraction of MO dye from wastewater. Several influencing extracting parameters such as concentration, effect of pH and others were evaluated. The nanoparticles of HAp were characterized by various techniques such as X-ray diffraction (XRD), Fourier transform infrared (FTIR) spectroscopy and scanning electron microscope (SEM). The developed extraction technique offered in this work could be a very promising as an alternative adsorbent for MO removal from industrial wastewater.

2. Materials and methods

2.1. Materials

All reagents and solvents used in this work were purchased for Aldrich and used as received without any further purification. Calcium nitrate $Ca(NO_3)_2{\cdot}4H_2O$ (99%), PEG 1000, ammonium hydrogen phosphate $(NH_4)_2{\cdot}HPO_4$ (99%). Distilled water was used throughout all the experiments. MO dye was also obtained from Sigma-Aldrich.

2.2. Solutions of MO

The MO model structure is shown in Fig. 1, taken as a pollutant model, it was used without purification. The MO

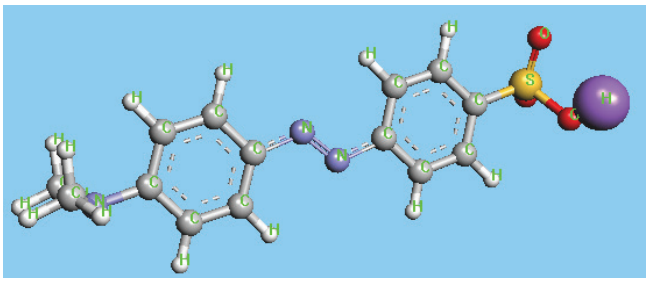

Fig. 1. Chemical structure of methyl orange (MO).

solutions were prepared by dissolving known quantities of the dye in doubly distilled water.

2.3. Synthesis of adsorbent in powder form

The nano-HAp was prepared by wet chemical method using $Ca(NO_3)_2{\cdot}4H_2O$ and $(NH_4)_2{\cdot}HPO_4$, as Ca and P precursors, respectively. To an aqueous solution of $Ca(NO_3)_2{\cdot}4H_2O$ (11.76 g) in 100 mL water was added dropwise, then an aqueous solution of $(NH_4)_2{\cdot}HPO_4$ (4.06 g) with stirring. The molar ratio of calcium to phosphorous was about 1.67. Then, PEG 1000 was added in an amount equal to 10% of the sum weight of the other two materials. The mixture was stirred for 10 min, then an ammonium solution (25%) was added dropwise to adjust the pH of the reaction solution to 10.5. The reaction mixture was heated at 90°C for 1 h. Then, it was stirred for 120 min at room temperature. The resulting precipitate was filtered and dried in an oven at 323 K to produce a fine powder [17]. Precipitated particles of nano-HAp were aged for 24 h at room temperature and then calcinated at 900°C for 2 h.

2.4. Adsorbent characterization

The purity and crystallinity of the nano-HAp adsorbents were determined by powder XRD using a rich Siefert 3000 diffractometer (Seifert, Germany) with Cu Ka1 radiation (λ = 1.5418 Å). The FTIR was performed using a Schimadzu FTIR 300 series instrument (Shimadzu Scientific Instruments) in the region of 400–4,000 cm^{-1} with 2 cm^{-1} resolution and 10 scans. The test samples were prepared by mixing 0.98 g of composite together with 0.02 g of KBr and converted to pellet. The morphology of the prepared adsorbent was characterized by emission-scanning electron microscopy, the filler/matrix interface was determined by using an SU 8020, 3.0 KV SE (U). The specimens were frozen under liquid nitrogen, fractured, mounted, coated with gold/palladium and observed using an applied tension of 10 kV.

2.5. Adsorption experiments

The experimental parts were performed using various concentrations of MO in 100 mL of water and using different amounts of adsorbent nanohydroxyapatite. All adsorption measurements were performed at 460 nm using UV–Vis spectrophotometer (PerkinElmer, Model 550S with a 1 cm path length), several factors were evaluated like temperatures, contact time, dose, adsorption isotherm, kinetics and thermodynamics. Before the adsorbate concentration was measured in solution, a calibration curve was prepared using a range of MO from 0 to 300 mg/L. All diluted solutions of MO were prepared from a stock solution with a concentration of 1,000 mg/L by dilution using double distilled water.

The removal ratio percentage (R, %) was calculated using Eq. (1):

$$R(\%) = \frac{C_0 C_f}{C_0} 100 \quad (1)$$

where C_0 is the initial concentration of MO and C_f is the final concentration of MO. All experiments were carried out in duplicates and the means were taken unless there is a difference of more than 5% between the readings then a third measurement was taken.

The effect of contact time was carried at 298, 313 and 323 K at different concentrations (3.27, 16.35 and 32.35 mg/L) using the time range from 5 to 50 min. The adsorption capacity was calculated according to Eq. (2):

$$Q_e = \frac{C_0 - C_e}{m} V \quad (2)$$

where Q_e is the amount of dye adsorbed per unit weight of adsorbent (mg/g). C_e is the equilibrium concentration of dye solution (mg/L), C_0 is the initial concentration of dye, m is the mass of nano-HAp (mg) used and V is the volume of solution in L.

2.6. Statistical analysis of results

As mentioned earlier all experiments were conducted in replicate, the mean was taken for each duplicate. In this study, the coefficient of variance was mostly less than 1%. The error range was determined using a certainty interval of 95%, which was used, for the data analysis by Excel Microsoft software by t test. All variations were considered statistically when $p < 0.05$ for the analysis of t test.

3. Results and discussion

3.1. Adsorbent characterization

The characterization results by XDR, SEM and FTIR of nano-HAp adsorbents are shown in Fig. 2.

The crystalline structure of the nano-HAp particles was identified using XDR. The XDR pattern of HAP diffraction peaks could be indexed to a single phase of HAp with a hexagonal structure (JCPDS no. 09-0432). The diffraction peaks with a 2θ values of 25.9, 31.8, 32.3, 32.9, 34.1 and 39.8 are corresponding to (002), (211), (300), (202) and (310) crystal face of nano-HAp, respectively. The XDR patterns indicate that, the nano-HAp has highly crystallized single phase as shown in Fig. 2(a).

The FTIR spectra of nano-HAp are shown in Fig. 2(b). The bands at 3,572 and 632 cm^{-1} are attributed to the stretching vibration and the deformation of mode of O–H, respectively, the bands at 1,089, 1,045 and 962 cm^{-1} are corresponding to the asymmetric phosphate stretching vibration of P–O in the phosphate group. The bands at 601 and 570 cm^{-1} are characteristics of the phosphate. From the IR analysis, the precipitated powders are proved to be HAp in nature. The presence of polyethylene glycol in HAp does not play any role in the structural deformation of HAp, meaning that nano-HAp crystallites were prepared.

SEM and TEM techniques were used in order to further confirm the surface modification of nano-HAp. The obtained SEM image is for nano-HAp for modified with polyethylene glycol in Figs. 2(c) and (d). The small particles are agglomerated with an average diameter of 180–170 nm. The figure also shows pores, these pores are beneficial for the circulation of the physiological fluid throughout the coatings when it is used as a biomaterial in bone implantation, also could be beneficial for adsorption. The pure nano-HAp sintered

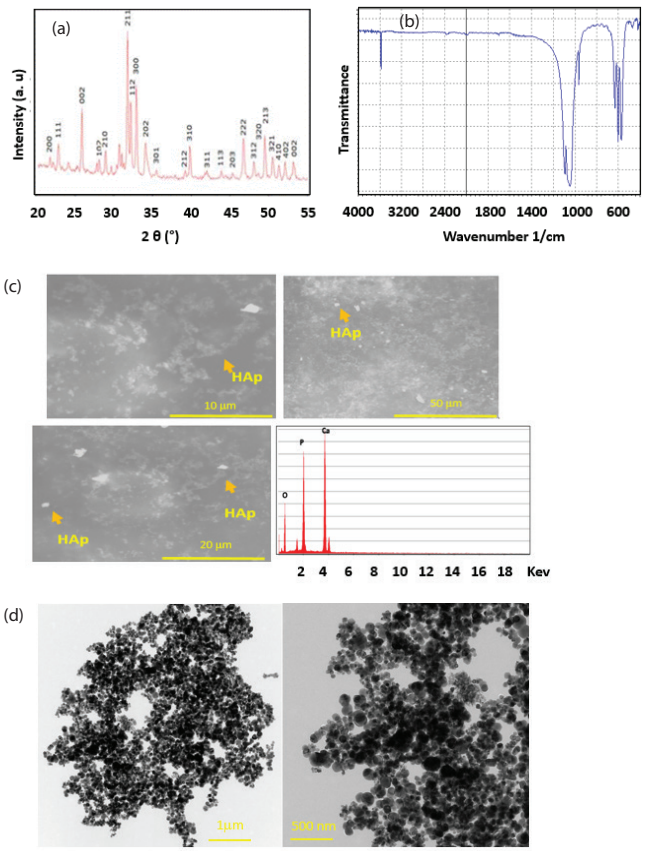

Fig. 2 (a) The XRD patterns of the bare HAp. (b) The FTIR spectra of the bare HAp. (c) The SEM images of the bare HAp and X-ray spectra of HAp (at What magnifications). (d) The TEM images of the HAp.

at 900°C for 2 h in stagnant air exhibits the morphology of clusters of grains structure as shown in Figs. 2(c) and (d), the powder modifier by PEG 1000 obtained after heat treatment at 900°C for 2 h, of the morphology of agglomerated grains.

3.2. The impact of contact time and concentration on adsorption

The quantities of methylene orange which is adsorbed (Q_t) at different concentration (3.27, 16.35 and 32.35 mg/L) and different contact times (5–45 min) were studied, and the results are shown in Fig. 3.

The MO adsorption on the nano-HAp samples were very fast in the first 5–15 min and reached the plateau after about 30 min at 298 and 313 K, the adsorption leveled off at after about 44 min. However, at T = 323 K, the adsorption continue to increase with time. As shown in Fig. 3, the highest rate of adsorption was obtained at 323 K.

The high rate of adsorption could be attributed to the high number of MO binding sites available on the surfaces of nano-HAp substrates and due to the high activation energies, which have been calculated in the thermodynamics section. The slow subsequent step (5–30 min) was due to the rearrangement of MO molecules to find available adsorption sites on the nano-HAp. Also, from Fig. 3, the equilibrium adsorption capacity increased from 5 to 17 mg/g for HAp as we increased the concentration from 3 to 32 mg/L. So, when the initial concentration

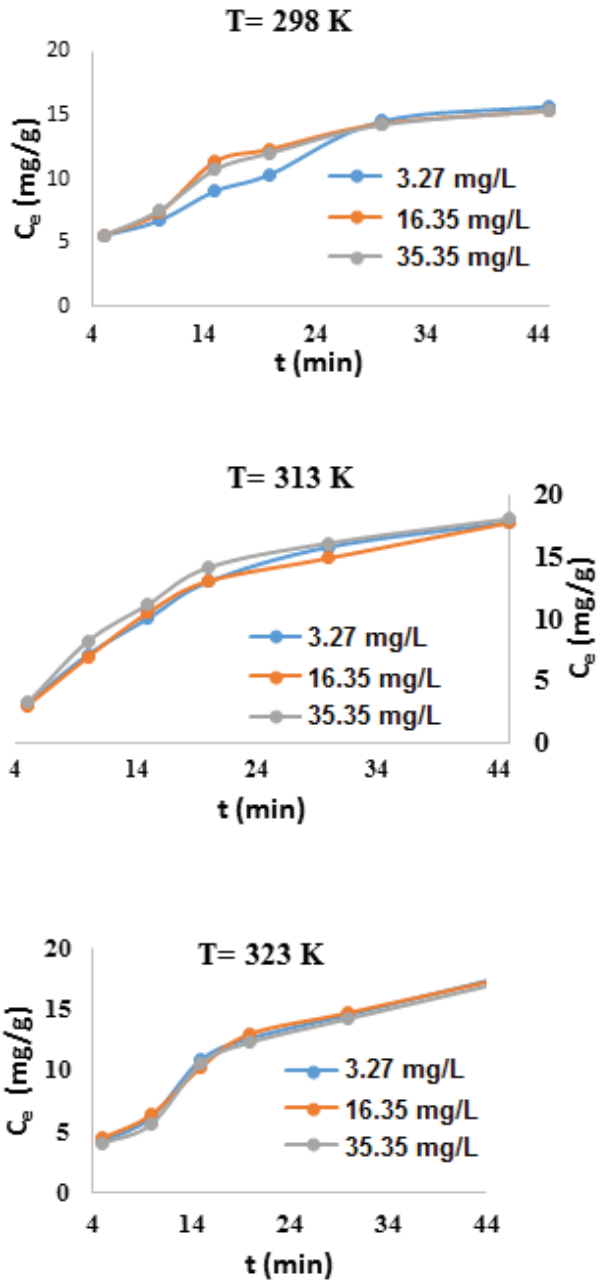

Fig. 3. Effect of contact time on the adsorption capacity of MO and temperature at different concentrations of MO.

increased, the mass transfer driving force will accelerate the MO ions diffusion from the bulk solution to nano-HAp surfaces and this will increase the equilibrium adsorption capacity [31,32]. In this study, a contact time of 150 min was used in studying the dose on adsorption efficiency.

3.3. Impact of adsorbent dose on extraction of MO

To evaluate the impact of adsorbent dose on the rate of removal of MO from water several experiments were carried out using various doses of nano-HAp ranging from 5 to 300 mg/L, and the results are summarized in Fig. 4.

This experiment was carried out using 100 mg/L solution of MO at 298, 313 and 323 K. From graphs shown in Fig. 4, the adsorption efficiency increases as the dosage increased. This is due to increase of vacant sites and the unsaturation of adsorption sites. Also, at 12 mg/L the three concentrations showed the same percentage of removal which means the vacant sites are almost saturated with MO ions.

3.4. The impact of pH value

The studied impact of pH on the MO adsorption on the HAp showed dramatic effect. And the impact was studied over the range of 2.0–12. The results are shown in Fig. 5. All of the HAp showed very high removal of MO at high pH 12. The percentage of removal reached almost 91% for the HAp at pH of 12. The active sites of HAp compounds were almost empty at the beginning and by the removal of MO start filling those sites. Also, it depends on the chemistry of solutes in the solution. At higher pH the active sites of HAp carries negative charge and the MO are cations which cause an electrostatic force and this will attract most of MB cations from the solution. There also may be else type of adsorption, for example, ion-exchange.

The point of zero charge is the pH at which the surface of adsorbent is globally neutral, that is, contains as much positively charged as negatively charged surface functions. Below this value, the surface is positively charged; beyond this value, it is negatively charged. So normally, it is always easier to adsorb a cation on a negatively charged surface, and an anion on a positively charged surface. However, other interactions may be stronger than purely electrostatic forces, making the effect of surface charge not so important. Additionally, a cation is often complexed with ligands, some of them being possibly negatively charged. Therefore, such a case, the cations are in fact a negative complex, which may adsorb very well on a positively charged surface.

In order to better comprehend the net charge of the adsorbent surface at the various pH solutions, the point zero charge (pH_{ZPC}) of the bone samples were measured. The results of pH_{ZPC} determination are shown in Fig. 6. The pH_{ZPC}, ZPC is defined as the pH at which the total surface charges become zero, of all bone samples showed the same behavior. The modified samples indicate a lower pH_{ZPC} of the HAp were estimated to be about 7.32 and 6.12, respectively, in comparison with unmodified bone (pH_{ZPC} = 7.8), which confirm that the surface of the pristine bone has been changed after chemical modification.

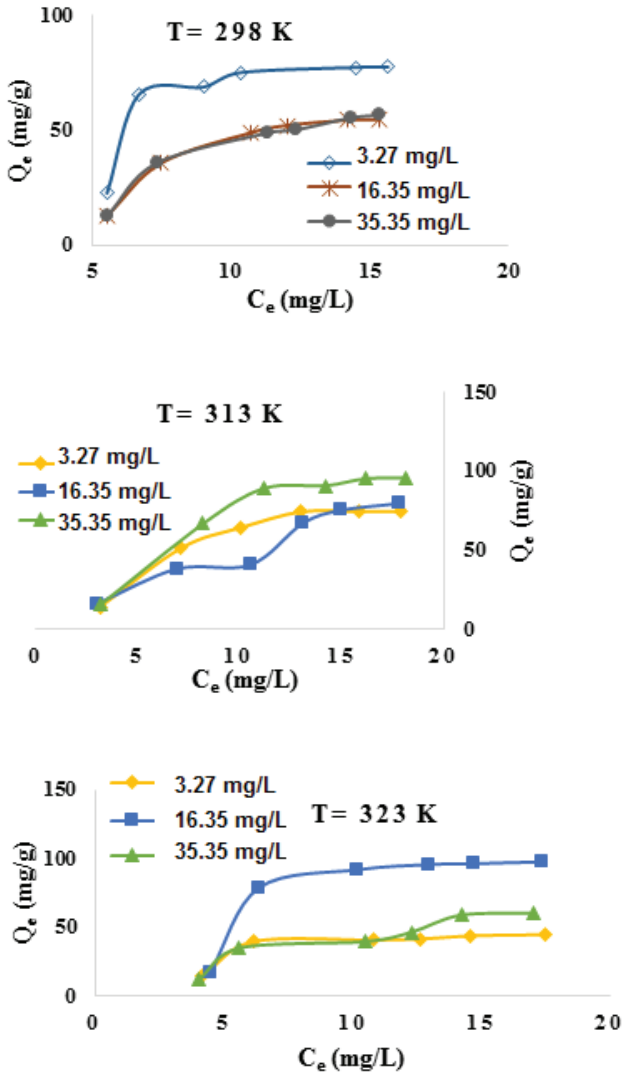

Fig. 4. Effect of adsorbent dosage on the removal of MO by HAp.

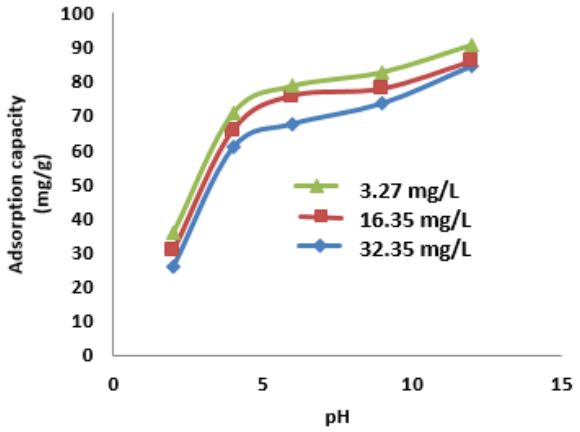

Fig. 5. Effect of pH on the adsorption of MO onto HAp at concentration of 10 mg/L, t = 50 min and T = 325 K.

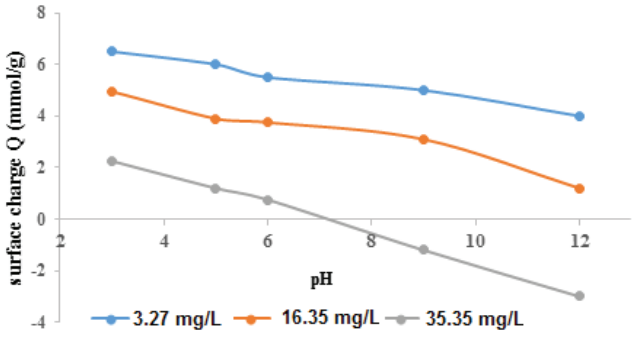

Fig. 6. Zeta potential of the bone sample of MO by HAp.

3.5. Adsorption isotherm

The adsorption equilibrium between the concentration of MO in liquid phase and the nano-HAp particles were determined using two adsorption isotherm models. Langmuir isotherm based on the kinetic principle and it describes the monolayer surface adsorption on the solid with definite localized sites that are energetically identical [33]. The model assumes that the adsorbate molecules can only accumulate only one localized site without lateral interaction between the adsorbed molecules, even on the nearby sites. Also, it assumes that no further adsorption can occurs after equilibrium. This model is shown in the following equation:

$$\frac{C_e}{Q_e} = \frac{1}{q_{\max}} C_e + \frac{1}{q_{\max} K_L} \tag{3}$$

where C_e is the equilibrium concentration of MO (mg/L), Q_e is the amount of adsorbate adsorbed per unit mass of nano-HAp at equilibrium (mg/g), $Q_{\max}$ is the theoretical maximum monolayer adsorption capacity of the adsorbent (mg/g) and K_L is the Langmuir isotherm constant related to the adsorption energy (L/mg).

From Langmuir isotherm, also it could be predicted if the adsorption is favorable or not using the dimensionless constant separation factor in Eq. (4):

$$R_L = \frac{1}{1 + K_L C_0} \tag{4}$$

where K_L is the Langmuir constant and C_0 is the initial adsorbate concentration. If R_L is greater than 1 it means the adsorption is not favorable. But if $0 < R_L < 1$ it means the adsorption is favorable and of course if $R_L = 1$ means linear adsorption.

The second type of isotherm model used is Freundlich isotherm, which represents the non-ideal adsorption that includes heterogeneous surface energy system and reported in Eq. (5):

$$Q_e = K_F C_e^{1/n} \tag{5}$$

where K_F (L/mg) is the Freundlich constant, $1/n$ is the adsorption intensity and if $(0.1 < 1/n < 0.5)$ the adsorption is favorable and if $(1/n > 2)$ means unfavorable.

All fitting parameters using the equations are listed in Table 1 and Figs. 7 and 8. From the values of the correlation coefficients (>0.99) and the separation factor R_L which was calculated for all the nano-HAp substrates $(0 < R_L < 1)$ while the values of $1/n$ were between 0.4746, 0.3165 and 0.3242 at T = 298 K; 0.4562, 0.4046 and 0.2562 at T = 313 K; 0.4368, 0.2892 and 0.4406 at T = 323 K, which indicates high adsorption intensity, that the adsorption approach conformed to Langmuir isotherm model (5). This indicates that all the functional groups of MO are equally and homogeneously spread over the outer porous surfaces of all HAp substrates.

3.6. Kinetics adsorption of MO on the nano-HAp

The adsorption kinetics of MO on the nano-HAp samples were studied for each nano-HAp adsorbate at four various concentrations of 3.27, 16.35 and 32.7 mg/L. The dynamic experimental data were fitted for pseudo-first-order, pseudo-second-order and the intraparticle diffusion model using the following equations [34]:

$$\ln(q_e - q_t) = \ln q_e - K_1 t \tag{6}$$

$$\frac{t}{q_t} = \frac{1}{K_{2q_e^2}} = \frac{t}{q_e} \tag{7}$$

$$Q_t = K_{\mathrm{id}} t^{1/2} + Z \tag{8}$$

$$\ln \frac{K(T_2)}{K(T_1)} = \frac{Ea}{R}\left(\frac{1}{T_1} - \frac{1}{T_2}\right) \tag{9}$$

where Q_e and Q_t are adsorption capacities (mg/g) at equilibrium and at different time t (min), respectively, K_1 is the pseudo-first-order rate constant (min^{-1}), K_2 is the pseudo-second-order rate constant (g/mg min). The K_{id} is the intraparticle diffusion rate constant ($\mathrm{mg\ g^{-1}\ min^{-1/2}}$) and Z (mg/g) which gives information about the thickness of boundary layer.

The values of all these parameters are shown in Tables 2 and 3 and Figs. 10 and 11. The value of K_1 was obtained by plotting $\ln(Q_e - Q_t)$ vs. t (Fig. 9); while K_2 and the adsorption capacity Q_e where calculated from the slope and the intercept

Table 1
Langmuir and Freundlich parameters for the adsorption of MO onto HAp

T (K)		298			313			323		
C_0 (mg/L)		3.27	16.35	32.35	3.27	16.35	32.35	3.27	16.35	32.35
Langmuir isotherm	Q^0 (mg/g)	87.719	105.26	87.719	94.3396	126.58	113.63	48.3091	116.27	85.47
	K_L (L/mg)	0.4810	0.0753	0.4810	0.2241	0.082	0.2829	0.6160	0.3282	0.1191
	R_L	0.3886	0.4480	0.3886	0.5770	0.4275	0.0984	0.3317	0.1870	0.2060
	R^2	0.9951	0.9725	0.9951	0.9732	0.6909	0.957	0.9963	0.9973	0.8265
Freundlich isotherm	$1/n$	0.4746	0.3165	0.3242	0.4562	0.4046	0.2562	0.4368	0.2892	0.4406
	K_F (L/mg)	8.2561	1.781	1.7711	5.889	6.0263	5.5367	8.2658	5.662	4.5642
	R^2	0.8746	0.8394	0.8223	0.8902	0.961	0.9162	0.672	0.6642	0.8342

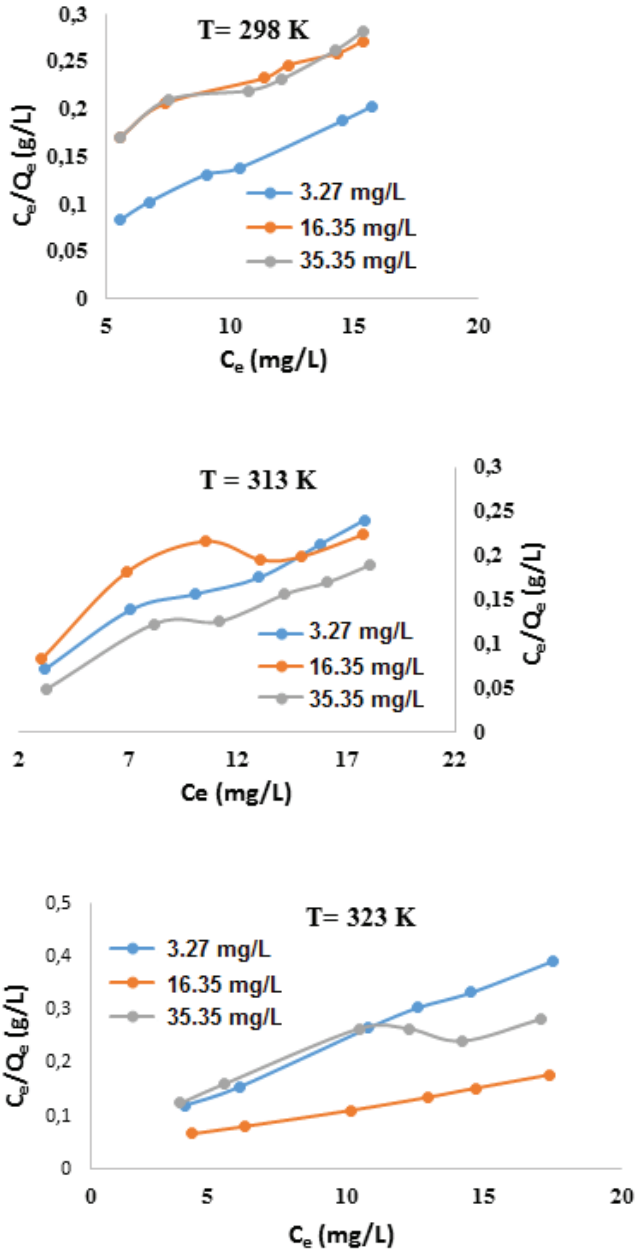

Fig. 7. Langmuir adsorption model fit of MO on HAp at different temperatures.

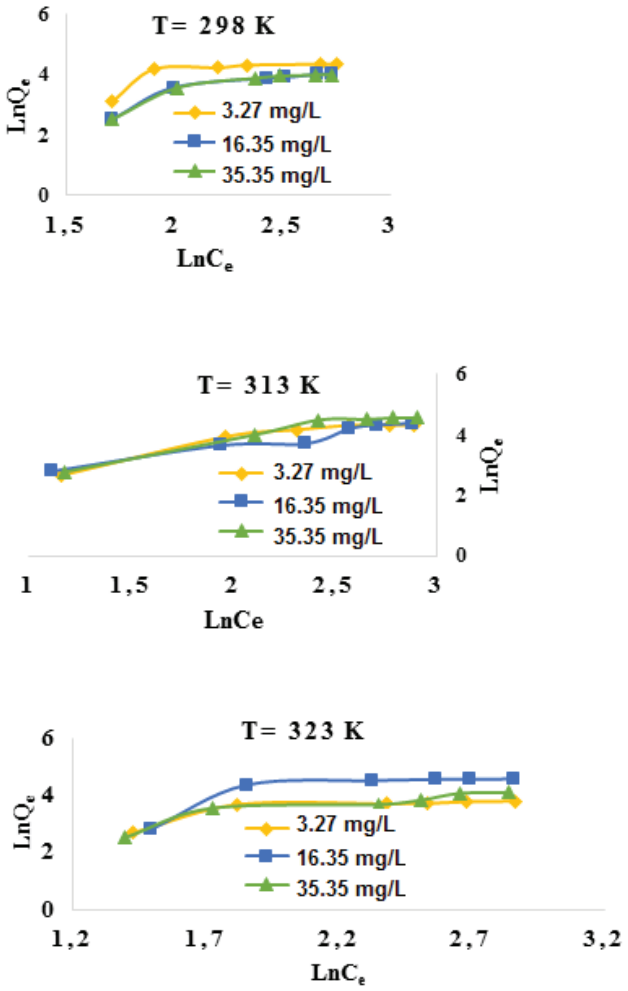

Fig. 8. Freundlich adsorption model fit of MO on HAp at different temperatures.

of plotting Q_t vs. t (Fig. 10). While K_{id} and Z obtained from plotting Q_t vs. $t^{1/2}$ (Fig. 11). When the experimental data were plotted for both the pseudo-first-order and the second-pseudo-order kinetics, the correlation coefficients (R^2) for the pseudo-second-order was higher than the pseudo-first-order and it reached 1 in most of the nano-HAp samples. Other indication also came from the calculated Q_e values for the pseudo-second-order were very close to the experimental Q_e values indicating that the adsorption process of MO on the surfaces of nano-HAp were followed and described by the pseudo-second-order (Table 2 and Fig. 9).

We studied the mechanism of the diffusion behavior of the adsorbed MO on nano-HAp samples at different concentrations (3.27, 16.35 and 32.35 mg/L) using the calculations and the theory proposed by Weber and Morris and the model, they suggested using Eq. (8).

From plotting Q_t vs. $t^{1/2}$ (Fig. 11), we can obtain the values of K_{id} and Z. The values are presented in Table 3. All plots were linear and did not passing through the origin indicating that the rate-limiting process is not the only rate-limiting step.

From Fig. 11, we see that for nano-HAp has first linear part, which represents the adsorption on the exterior surface or sometimes represents the instant adsorption stages. The rest of stages were also linear, and they were describing the gradual adsorption of MO and they showed the intraparticle diffusion rate-limiting steps. The nano-HAp showed different behavior and all of the plots where almost linear without two stages (Fig. 11) [35]. Other conclusion from the values of Z that they were increasing with the increase of concentration indicating augmentation in the density of outer layer and dwindling in external mass transfer [36] while the potential of internal mass transfer increased. Several studies showed the same behavior we obtained [37].

Table 2
The pseudo-second-order model for adsorption of different initial concentrations of MO by HAp

T (K)	298			313			323		
C_0 (mg/L)	K_2 (g/mg min)	Q_{cal} (mg/g)	R^2	K_2 (g/mg min)	Q_{cal} (mg/g)	R^2	K_2 (g/mg min)	Q_{cal} (mg/g)	R^2
3.27	4.518×10^{-3}	82.6446	0.999	1.91×10^{-3}	86.9561	0.9866	6.2×10^{-3}	48.3091	0.9965
16.35	1.72×10^{-3}	68.9655	0.9877	5.2318	112.359	0.976	1.42×10^{-3}	114.94	0.9668
32.25	2.51×10^{-3}	63.6942	0.9879	1.14×10^{-3}	116.279	0.9698	9.2825	80	0.9875

Table 3
Intraparticle diffusion for adsorption of different initial concentrations of MO by HAp

T (K)	298			313			323		
C_0 (mg/L)	K_{id}	Z	R^2	K_{id}	Z	R^2	K_{id}	Z	R^2
3.27	16.955	5.1341	0.9838	21.214	12.627	0.9941	9.3006	4.4579	0.9987
16.35	15.845	12.459	0.9949	24.722	28.686	0.9953	29.09	24.009	0.9844
32.35	14.242	6.3229	0.9886	32.401	40.01	0.9773	16.035	13.559	0.9931

Finally, the activation energy was calculated for the sorption process at 298 and 323 K, respectively, using Eq. (9). The idea is to see the impact of temperature on adsorption behavior of MO on nano-HAp. These values give an idea about the type of adsorption. In non-activated chemical sorption, the activation energy is close to zero and this is what we obtained. Usually low activation energy values suggest that the energy barrier toward ion adsorption is always easier to overcome and the adsorption process takes place very fast.

3.7. Adsorption thermodynamics

To understand the thermodynamics behavior of the adsorption of MO dye on HAp, the thermodynamics parameters like equilibrium rate constant K (L/g), the standard Gibbs free energy $\Delta G°$ (J/mol), the standard entropy $\Delta S°$ (J/mol/K) and the standard enthalpy $\Delta H°$ (J/mol) were determined at different temperatures T (K).

All of these parameters were calculated using Van't Hoffs equation (Eq. (9)) [23]:

$$\ln K_S = \frac{\Delta S}{R} - \frac{\Delta H}{RT} \tag{10}$$

$$\Delta G° = \Delta H° - T\Delta S° \tag{11}$$

The $\ln K_s$ vs. $1/T$ was plotted as shown in Fig. 10, the slopes and intercept represent the values of these parameters. The obtained values are shown in Table 4.

As shown in Table 4, the values of $\Delta S°$ and $\Delta H°$ are positive which denote that the entropy increased at the solid/solution interface through the adsorption process, while $\Delta H°$ values were positive for the HAp particles due to their endothermic nature [34,38–40].

In Table 4, the thermodynamic parameters for the adsorption of MO onto HAp ($C°$ = 3.27 mg/L) are given. Also, from the results we found all the free energies for the nano-HAp were negative indicating spontaneous nature of the adsorption process at different temperatures (Fig. 12).

The spontaneous nature of the adsorption process could be attributed to three possible ionic interactions between the two substances as shown in Fig. 13(B). The first two are related to the interaction between the Ca^{++} and Ca^{+} and sulfate ion. As shown in Fig. 13(A), MO has a resonance structure; the resonance structure has an ammonium group. The ammonium group undergoes interaction with the phosphate ions of HAp.

3.8. Desorption and regeneration

This part of experiment was carried out to determine number of times the adsorbents can be used and determine their efficiencies. The experiment was repeated four times using the same adsorbent and the results are summarized in Table 5 [41–46].

To evaluate the adsorption ability of the current adsorbent, a comparative study was made as shown in Table 5 between nano-HAp and several other nanomaterials published in the literature. It was found that the nano-HAp possesses a higher affinity for MO than most of the adsorbent reported in the literature.

From the whole cycles, we could not see any remarkable decrease in the sorption capacities. The desorption efficiency of MO was maintained almost the same thing in nano-HAp. From the magnetic field study (Fig. 14) it can be seen clearly that the used sorbent can be recycled easily from the wastewater using magnetic field. This will enhance the industrial application to avoid secondary pollution during the wastewater treatment.

This part of experiment was carried out to determine number of times the adsorbents can be used and determine their efficiencies. The experiment was repeated four times using the same adsorbent and the results are summarized in Table 6. From the whole cycles, we could not see any remarkable decrease in the sorption capacities. The desorption efficiency of MO was maintained almost the same thing in

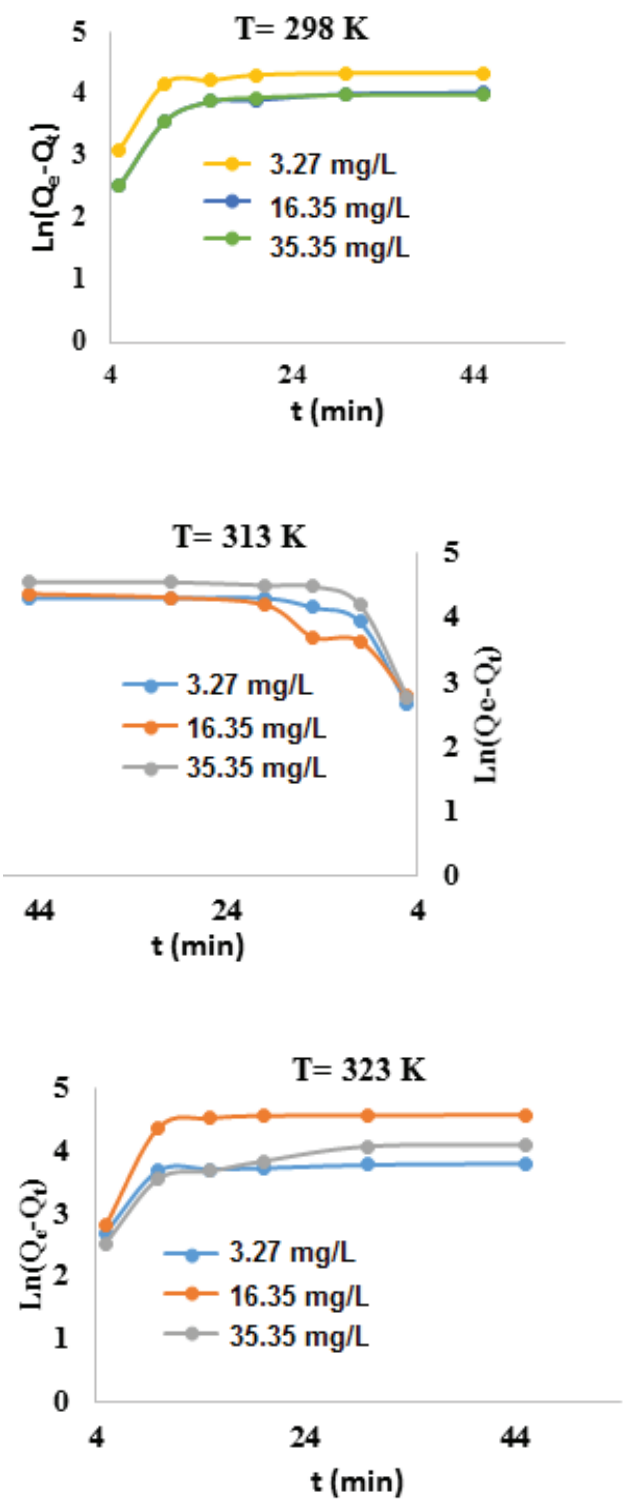

Fig. 9. Pseudo-first-order model for the adsorption of MO onto HAp.

MNCs. From the magnetic field study, it can be seen clearly that the used sorbent can be recycled easily from the wastewater using magnetic field. This will enhance the industrial application to avoid secondary pollution during the wastewater treatment.

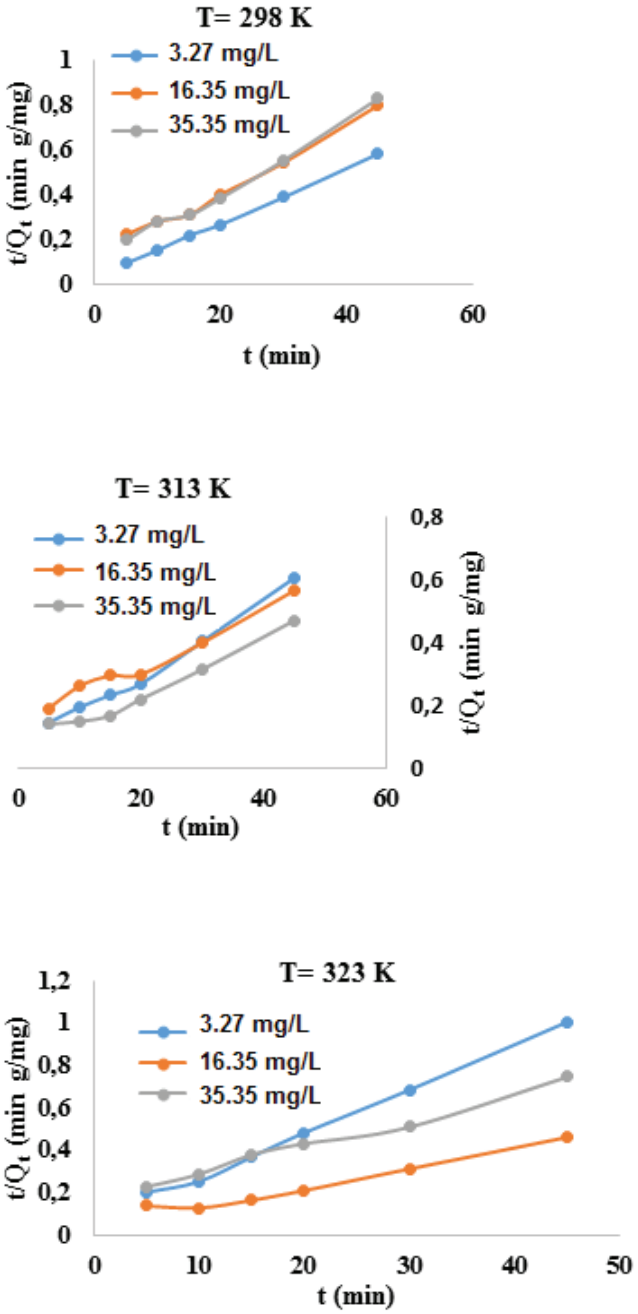

Fig. 10. Pseudo-second-order model for the adsorption of MO onto HAp.

4. Conclusion

In this study, we have successfully synthesized a novel nanohydroxyapatite adsorbent; the structure of the synthesized nano-HAp was confirmed by FTIR and SEM. The ability of the nano-HAp material to extract MO from wastewater was evaluated. Results showed that nano-HAp has a moderate efficiency toward MO. The rate of adsorption showed dependence on temperature and amount of nano-HAp. The effect of temperature on the rate of adsorption was noticeable in all runs, in the first 5–15 min of contact time nano-HAp showed the

highest rate of adsorption. The rate leveled after about 20 min of contact time at room temperature. However, at higher temperature the rate kept increasing for a longer period of time. The analysis results also show that, the adsorption efficiency increased as the dosage of nano-HAp increased which could be due to the availability of vacant sites and the unsaturation of adsorption sites. The value of the correlation coefficients (>0.99), the separation factor R_L (and the $1/n$ indicates high adsorption intensity). The adsorption mechanism was predicted by Langmuir isotherm model. When the experimental data were plotted for both the pseudo-first-order and the pseudo-second-order kinetics, the correlation coefficients (R^2) for the pseudo-second-order was higher than that for the pseudo-first-order and it reached 1 for all nano-HAp samples. The calculated Q_e values for the pseudo-second-order were very close to the experimental Q_e values indicating that the adsorption process of MO on the surfaces of nano-HAp, and were described by the pseudo-second-order. The $\Delta S°$ and $\Delta H°$ values for the adsorption

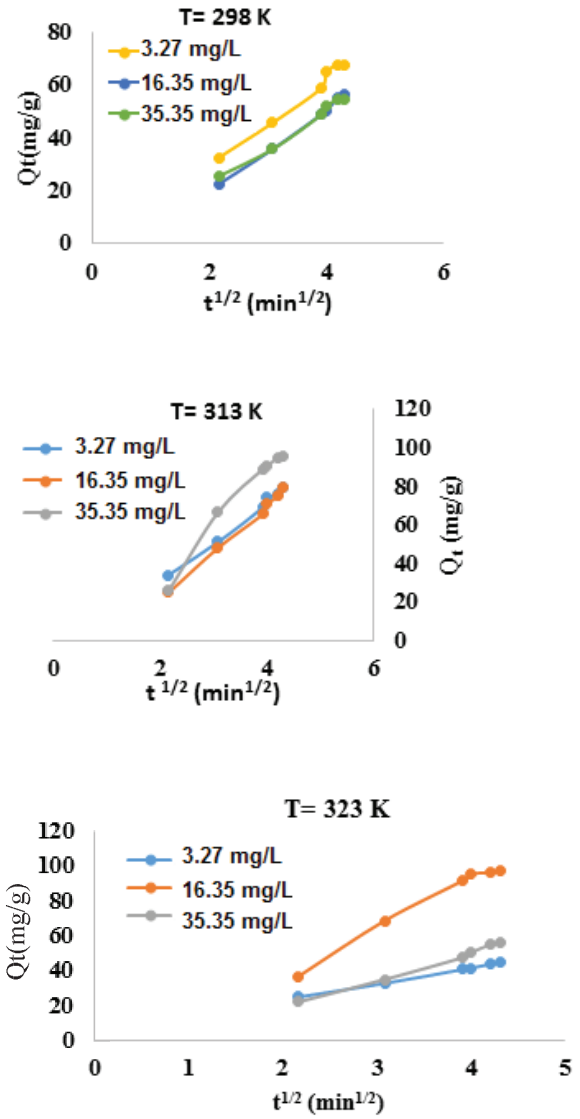

Fig. 11. Intraparticle diffusion model for the adsorption of MO onto HAp at many different concentrations.

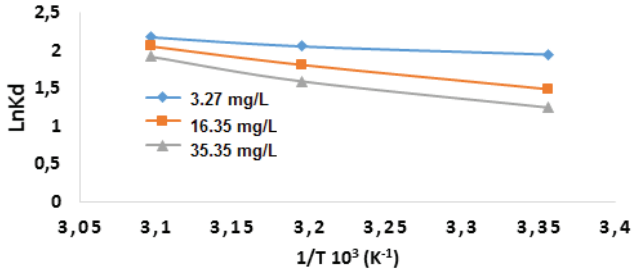

Fig. 12. Adsorption thermodynamics of MO onto HAp.

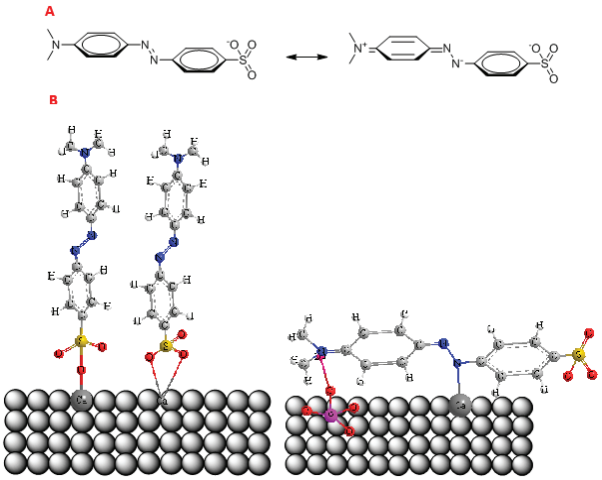

Fig. 13. A 3D scheme shows the possible interactions between nano-HAp and MO.

Table 4
Thermodynamic parameters for the adsorption of MO onto HAp

$C°$ (mg/L)	3.27			16.35			32.35		
T (K)	$\Delta G°$ (kJ/mol)	$\Delta H°$ (kJ/mol)	$\Delta S°$ (J/mol/K)	$\Delta G°$ (kJ/mol)	$\Delta H°$ (kJ/mol)	$\Delta S°$ (J/mol/K)	$\Delta G°$ (kJ/mol)	$\Delta H°$ (kJ/mol)	$\Delta S°$ (J/K mol)
298	–4.8087	7.1543	40.1448	–3.6761	1.8003	72.7509	–3.0466	21.2168	81.42118
313	–5.4199			–4.7673			–4.2679		
323	–5.8214			–55.4948			–5.0822		

Table 5
Comparison of the removal efficiency of MO by different adsorbents

Adsorbent	Q_m (mg/g)	Adsorbent dose (g/L)	Equilibrium time (min)	Adsorption condition	Reference
Surfactant-modified silkworm exuviate	87.3	2	60	pH = 7, T = 30.2°C	[35]
Rectorite/iron oxide nanocomposites	0.36	2	1	T = 25°C	[36]
SiO_2-coated Fe_3O_4 magnetic nanoparticles	53.19	1	30	pH = 2.66, T = 25°C	[37]
γ-Fe_2O_3/SiO_2/chitosan composite	34.49	1	300	T = 37°C	[38]
γ-Fe_2O_3 crosslinked chitosan composite	29.46	1	100	pH = 6.6, T = 27°C	[39]
Magnetic cellulose beads	1.47	250	180	pH = 7	[40]
γ-Fe_2O_3/2C nanocomposite	72.68	1	100	pH = 4.8, T = 25°C	This study
SWCNT-MO	454.545	0.01	20	pH = 7, T = 27°C	[41]
Poly HEMA–chitosan-MWCNT nanocomposite	306.1	0.3	180	pH = 4–10, T = 32°C	[42]
Graphene oxide	0.35	500		pH = 8, T = 25°C	[43]
MWCNT-COOH-MG	30	50	20	pH = 9, T = 55°C	[44]
Graphene oxide-MG	27.16	200	100	pH = 3, T = 25°C	[45]
Polyaniline/zirconium oxide	192.30	300	30	pH = 3, T = 26°C	[46]

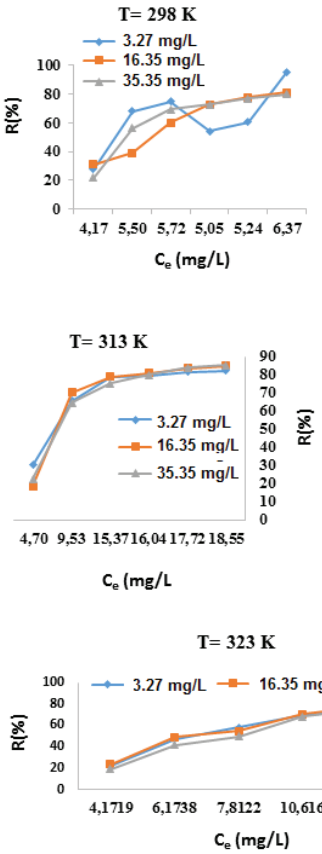

Fig. 14. Regeneration and desorption efficiencies for HAp samples.

Table 6
Percentage of MO dye removal by the regenerated adsorbent compared with a fresh one (temperature = 25°C, pH = 10, solution volume = 50 mL, adsorbent dose = 0.1 g, contact time = 50 min)

Recycling times	1	2	3	4
Cs (MO removal efficiencies, %)	98.8	98.6	98.5	98.2
NCS (MO removal efficiencies, %)	99.3	99.3	99.1	99.0
MNCs (MO removal efficiencies, %)	99.9	99.8	99.6	99.5

process were positive indicating that the randomness at the solid/solution interface increased during adsorption process, while $\Delta H°$ values were positive for the nano-HAp particles due to their endothermic nature. The free energies for the nano-HAp were negative indicating a spontaneous nature of the adsorption process at different temperatures.

Acknowledgments

The authors would like to thank both the Palestine Higher Education for their financial support and would like to thank the Arab Union Universities for their financial aid.

Symbols

HAp — Hydroxyapatite
nano-HAp — Nano-hydroxyapatite

MO	—	Methyl orange
R	—	Removal ratio percentage
Q_t	—	The adsorbed amount of MO at time t, mg/g
Q_e	—	The amount of adsorbate adsorbed per unit mass of nano-HAp at equilibrium, mg/g
Q_{max}	—	The theoretical maximum monolayer adsorption capacity of the adsorbent, mg/g
K_L	—	The Langmuir isotherm constant related to the adsorption energy, L/mg
$\Delta G°$	—	Gibbs free energy, J/mol
$\Delta S°$	—	Standard entropy, J/mol/K
$\Delta H°$	—	Standard enthalpy, J/mol

References

[1] S. Malato, P. Fernandez-Ibanez, M. Maldonado, J. Gernajak, Decontamination and disinfection of water by solar photocatalysis: recent overview and trends, Catal. Today, 147 (2009) 1–59.

[2] F. Sakr, A. Sennaoui, M. Elouardi, M. Tamimi, A. Assabbane, Adsorption study of Methylene Blue on biomaterial using cactus, J. Mater. Environ. Sci., 6 (2015) 397–406.

[3] I. Holme, Developments in the Chemistry and Technology of Organic Dyes, J. Griffiths, Ed., Ecological Aspects of Colour Chemistry, Society of Chemistry Industry, Oxford, 1984, p. 111–128.

[4] D. Georgiou, A. Aivazidis, J. Hatiras, Treatment of cotton textile wastewater using lime and ferrous sulfate, Water Res., 37 (2003) 2248–2250.

[5] G. Mascolo, R. Comparelli, M.L. Curri, Photocatalytic degradation of methyl red by TiO_2: comparison of the efficiency of immobilized nanoparticles versus conventional suspended catalyst, J. Hazard. Mater., 142 (2007) 130–137.

[6] M. Muthukumar, D. Sargunamani, M. Senthil Kumar, Studies on decolouration toxicity and possibility for recycling of acid dye effluents using ozone treatment, Dyes Pigm., 64 (2005) 39–44.

[7] H.Y. Shu, C.R. Huang, Degradation of commercial azo dye in water using ozonation and UV enhanced ozonation process, Chemosphere, 29 (1994) 2597–2607.

[8] M.H. Zhou, Q.H. Yu, C.C. Lei, Electro-Fenton method for the removal of methyl red in an efficient electrochemical system, Sep. Purif. Technol., 57 (2007) 380–387.

[9] P.C.C. Faria, J.J.M. Órfão, M.F.R. Pereira, Adsorption of anionic and cationic dyes on activated carbons with different surface chemistries, Water Res., 39 (2004) 1461–1470.

[10] N.C. Feitoza, T.D. Gonc, J.J. Mesquita, J.S. Menegucci, M.K.M.S. Santos, J.A. Chaker, R.B. Medeiros, A.M.M. Cunha, J.C. Rubim, M.H. Sousa, Fabrication of glycine-functionalized maghemite nanoparticles formagnetic removal of copper from wastewater, J. Hazard. Mater., 264 (2014) 153–160.

[11] S.S. Banerjee, D.H. Chen, Fast removal of copper ions by gum arabic modified magnetic nano-adsorbent, J. Hazard. Mater., 147 (2007) 792–799.

[12] M. Ozmen, K. Can, G. Arslan, A. Tor, Y. Cengeloglu, M. Ersoz, Adsorption of Cu(II) from aqueous solution by using modified Fe_3O_4 magnetic nanoparticles, Desalination, 254 (2010) 162–169.

[13] T. Burks, M. Avila, F. Akhtar, M. Göthelid, P.C. Lansåker, M.S. Toprak, M. Muhammed, A. Uheida, Studies on the adsorption of chromium (VI) onto 3-mercaptopropionic acid coated superparamagnetic iron oxide nanoparticles, J. Colloid Interface Sci., 425 (2014) 36–43.

[14] D. Singh, R.K. Gautam, R. Kumar, B.K. Shukla, V. Shankar, V. Krishna, Citric acid coated magnetic nanoparticles: synthesis, characterization and application in removal of Cd(II) ions from aqueous solution, J. Water Process Eng., 4 (2014) 233–241.

[15] C. Zhou, W. Zhang, M. Xia, W. Zhou, Q. Wan, K. Peng, B. Zou, Synthesis of poly(acrylic acid) coated-Fe_3O_4 superparamagnetic nano-composites and their fast removal of dye from aqueous, J. Nanosci. Nanotechnol., 13 (2013) 4627–4633.

[16] X. Qu, P.J.J. Alvarez, Q. Lim, Applications of nanotechnology in water and wastewater treatment, Water Res., 47 (2013) 3931–3946.

[17] K. Azzaoui, M. Berrabah, E. Mejdoubi, A. Lamhamdi, A. Elidrissi, B. Hammouti, Use of hydroxylapatite composite membranes for analysis of bisphenol A, Res. Chem. Intermed., 40 (2013) 2621–2628.

[18] B. Razzouki, S. El Hajjaji, K. Azzaoui, A. Errich, A. Lamhamdi, M. Berrabah, L. Elansari, Physicochemical study of arsenic removal using iron hydroxide, J. Mater. Environ. Sci., 6 (2015) 144–1450.

[19] K. Azzaoui, A. Lamhamdi, E. Mejdoubi, B. Hammouti, M. Berrabah, Synthesis of hydroxyethylcellulose and hydroxyapatite composite for analysis of bisphenol A, Arabian J. Chem. Environ. Res., 1 (2014) 41–48.

[20] K. Azzaoui, B. Hammouti, A. Lamhamdi, E. Mejdoubi, M. Berrabah, A. Elidrissi, M.M.G. Fouda, S.S. Al-Deyab, Structure and properties of hydroxyapatite/hydroxyethyl cellulose acetate composite film, Carbohydr. Polym., 115 (2015) 170–176.

[21] A. Lamhamdi, K. Azzaoui, E. Mejdoubi, B. Hammouti, M Berrabah, M. Zegmout, B. Razzouki, Contribution of adsorption of metals using calcium phosphates in the presence of support polyethylene glycol, J. Mater. Environ. Sci., 5 (2014) 2584–2589.

[22] K. Azzaoui, A. Lamhamdi, E. Mejdoubi, M. Berrabah, B. Hammouti, A. Elidrissi, M.M.G. Fouda, S.S. Al-Deyab, Synthesis and characterization of composites based on cellulose acetate and hydroxyapatite application to the absorption of harmful substrate, Carbohydr. Polym., 111(2014) 41–46.

[23] M.K. Khan, L. Wu, M.N. Mondal, Z. Yao, L. Ge, T. Xu, Adsorption of methyl orange from aqueous solution on anion exchange membranes: adsorption kinetics and equilibrium, Membr. Water Treat., 7 (2016) 23–38.

[24] N.P. Smirnova, N.I. Surovtseva, T.V. Fesenko, E.M. Demianenko, A.G. Grebenyuk, A.M. Eremenko, Photodegradation of dye acridine yellow on the surface of mesoporous TiO_2, SiO_2/TiO_2 and SiO_2 films: spectroscopic and theoretical studies, J. Nanostruct. Chem., 5 (2015) 333–346.

[25] T.A. Devi, N. Ananthi, T.P. Amaladhas, Photobiological synthesis of noble metal nanoparticles using *Hydrocotyle asiatica* and application as catalyst for the photodegradation of cationic dyes, J. Nanostruct. Chem., 6 (2016) 75–92.

[26] M. Sadiq, A. Nesaraj, Soft chemical synthesis and characterization of $BaWO_4$ nanoparticles for photocatalytic removal of Rhodamine B present in water sample, J. Nanostruct. Chem., 5 (2015) 45–54.

[27] H. Tavakkoli, T. Moayedipour, Fabrication of perovskite-type oxide $La_{0.5}Pb_{0.5}MnO_3$ nanoparticles and its dye removal performance, J. Nanostruct. Chem., 4 (2014) 116–225.

[28] A. Abbasi, J.J. Sardroodi, Theoretical study of the adsorption of NO_x on TiO_2/MoS_2 nanocomposites: a comparison between undoped and N-doped nanocomposites, J. Nanostruct. Chem., 6 (2016) 309–327.

[29] K. Zare, V.K. Gupta, O. Moradi, A.H. Makhlouf, M. Sillanpää, M.N. Nadagouda, H. Sadegh, R. Shahryari-ghoshekandi, A. Pal, Z. Wang, I. Tyagi, M. Kazemi, A comparative study on the basis of adsorption capacity between CNTs and activated carbon as adsorbents for removal of noxious synthetic dyes: a review, J. Nanostruct. Chem., 5 (2015) 227–236.

[30] N. Akartasse, E. Mejdoubi, B. Razzouki, K. Azzaoui, S. Jodeh, O. Hamed, M. Ramdani, A. Lamhamdi, M. Berrabah, I. Lahmass, W. Jodeh, S. E.L. Hajjaji, Natural product based composite for extraction of arsenic (III) from waste water, Chem. Cent. J., 11 (2017) 33. PDOI 10.1186/s13065-017-0261-9.

[31] V. Vadivelan, K.V. Kumar, Equilibrium, kinetics, mechanism, and process design for the sorption of methylene blue onto rice husk, J. Colloid Interface Sci., 286 (2005) 90–100.

[32] G. Limousin, J.-P. Gaudet, L. Charlet, S. Szenknect, V. Barthès, M. Krimissa, Sorption isotherms: a review on physical bases, modeling and measurement, Appl. Geochem., 22 (2007) 249–275.

[33] S. Jodeh, J. Amarah, S. Radi, O. Hamed, I. Warad, R. Salghi, A. Chetouni, S. Samhan, R. Alkowni, Removal of methylene blue from industrial wastewater in Palestine using polysiloxane surface modified with bipyrazolic tripodal receptor, Moroccan J. Chem., 4 (2016) 140–156.

[34] H. Guo, S. Zhang, Z. Kou, S. Zhai, W. Ma, Y. Yang, Removal of cadmium(II) from aqueous solutions by chemically modified maize straw, Carbohydr. Polym., 115 (2015) 177–185.
[35] L. Wang, J. Zhang, R. Zhao, C. Li, Y. Li, C. Zhang, Adsorption of basic dyes on activated carbon prepared from *Polygonum orientale* Linn: equilibrium, kinetic and thermodynamic studies, Desalination, 254 (2010) 68–74.
[36] K.A.G. Gusmão, L.V.A. Gurgel, T. Melo, L.F. Gil, Application of succinylated sugarcane bagasse as adsorbent to remove methylene blue and gentian violet from aqueous solutions – kinetic and equilibrium studies, Dyes Pigm., 92 (2012) 967–974.
[37] O. Moradi, M. Aghaie, K. Zare, M. Monajjemi, H. Aghaie, The study of adsorption characteristics Cu^{2+} and Pb^{2+} ions onto PHEMA and P(MMA-HEMA) surfaces from aqueous single solution, J. Hazard. Mater., 170 (2009) 673–679.
[38] O. Moradi, K. Zare, M. Monajjemi, M. Yari, H. Aghaie, The studies of equilibrium and thermodynamic adsorption of Pb(II), Cd(II) and Cu(II) ions from aqueous solution onto SWCNTs and SWCNT–COOH surfaces, Fullerenes Nanotubes Carbon Nanostruct.,18 (2010) 285–302.
[39] S. Parlayici, V. Eskizeybek, A. Avcı, E. Pehlivan, Removal of chromium (VI) using activated carbon-supported-functionalized carbon nanotubes, J. Nanostruct. Chem., 5 (2015) 255–263.
[40] M. Anbia, M. Khoshbooei, Functionalized magnetic MCM-48 nanoporous silica by cyanuric chloride for removal of chlorophenol and bromophenol from aqueous media, J. Nanostruct. Chem., 5 (2015) 139–146.
[41] M.S. Derakhshan, O. Moradi, The study of thermodynamics and kinetics methyl orange and malachite green by SWCNTs, SWCNT-COOH and SWCNT-NH_2 as adsorbents from aqueous solution, J. Ind. Eng. Chem., 20 (2014) 3186–3194.
[42] H. Mahmoodian, O. Moradi, B. Shariatzadeh, A. Tawfik, I. Salehf, Tyagi, A. Maity, M. Asif, V.K. Gupta, Enhanced removal of methyl orange from aqueous solutions by poly HEMA–chitosan-MWCNT nano-composite, J. Mol. Liq., 202 (2015) 189–198.
[43] D. Robati, B. Mirza, M. Rajabi, O. Moradi, I. Tyagi, S. Agarwal, V.K. Gupta, Removal of hazardous dyes-BR 12 and methyl orange using graphene oxide as an adsorbent from aqueous phase, Chem. Eng. J., 284 (2016) 687–697.
[44] D. Robati, M. Rajabi, M. Moradi, F. Najafi, I. Tyagi, S. Agarwal, V.K. Gupta, Kinetics and thermodynamics of malachite green dye adsorption from aqueous solutions on graphene oxide and reduced graphene oxide, J. Mol. Liq., 214 (2016) 259–263.
[45] D. Robati, B. Mirza, R. Ghazisaeidi, M. Rajabi, O. Moradie, I. Tyagif, S. Agarwalg, V.K. Gupta, Adsorption behavior of methylene blue dye on nanocomposite multi-walled carbon nanotube functionalized thiol (MWCNT-SH) as new adsorbent, J. Mol. Liq., 216 (2016) 830–835.
[46] S. Agarwal, I. Tyagi, V.K. Gupta, F. Golbaz, A.N. Golikand, O. Moradi, Synthesis and characteristics of polyaniline/zirconium oxide conductive nanocomposite for dye adsorption application, J. Mol. Liq., 218 (2016) 494–498.